



1 Wet-dry cycles impact DOM retention in subsurface soils

2 Olshansky Yaniv, Robert A. Root, Jon Chorover

3 Department of Soil, Water and Environmental Science, University of Arizona, Tucson, 85721, USA

4 *Correspondence to:* (Yaniv Olshansky yanivo@email.arizona.edu)

5 **Abstract.** Transport and reactivity of carbon in the critical zone are highly controlled by reactions of dissolved
6 organic matter (DOM) with subsurface soils, including adsorption, transformation and exchange. These reactions
7 are dependent on frequent wet-dry cycles common to the unsaturated zone, particularly in semi-arid regions. To
8 test for an effect of wet-dry cycles on DOM interaction and stabilization in subsoils, samples were collected from
9 subsurface (Bw) horizons of an Entisol and an Alfisol from the Catalina-Jemez Critical Zone Observatory and
10 sequentially reacted (four batch steps) with DOM extracted from the corresponding soil litter layers. Between each
11 reaction step, soils either were allowed to air dry (“wet-dry” treatment) before introduction of the following DOM
12 solution or were maintained under constant wetness (“continually-wet” treatment). Microbial degradation was the
13 dominant mechanism of DOM loss from solution for the Entisol subsoil, which had higher initial organic C content,
14 whereas sorptive retention predominated in the lower C Alfisol subsoil. For a given soil, bulk dissolved organic C
15 losses from solution were similar across treatments. However, a combination of Fourier transform infrared (FTIR)
16 and near edge X-ray absorption fine structure (NEXAFS) spectroscopic analyses revealed that wet-dry treatments
17 enhanced the interactions between carboxyl functional groups and soil particle surfaces and scanning transmission
18 X-ray microscopy (STXM) data suggested that cation bridging by Ca^{2+} was the primary mechanism for carboxyl
19 association with soil surfaces. STXM data also showed that spatial fractionation of adsorbed OM on soil organo-
20 mineral surfaces was diminished relative to what might be inferred from previously published observations
21 pertaining to DOM fractionation on reaction with specimen mineral phases. This study provides direct evidence of
22 the role of wet-dry cycles in affecting sorption reactions of DOM to a complex soil matrix. In the soil environment,
23 where wet-dry cycles occur at different frequencies from site to site and along the soil profile, different interactions
24 between DOM and soil surfaces are expected and needs to be consider for the overall assessment of carbon
25 dynamics.



26 1 Introduction

27 Dissolved organic matter (DOM) is the main vehicle of organic carbon and nutrient transport to the subsoil (Kaiser
 28 and Kalbitz, 2012; Kalbitz et al., 2000). There it stimulates key biogeochemical processes including heterotrophic
 29 microbial activity (Fontaine et al., 2007), mineral transformation, and organic and inorganic nutrient and
 30 contaminant mobilization (Chorover et al., 2007; Polubesova and Chefetz, 2014; Zhao et al., 2011). Interactions
 31 with subsoil surfaces act to stabilize DOM against advective transport and microbial degradation (Eusterhues et al.,
 32 2014; Kalbitz et al., 2000; Lutzow et al., 2006). Furthermore, prior studies have shown that DOM generated in the
 33 surface litter layers can be transported preferentially to clay-enriched subsoils via macropore flow paths that bypass
 34 the intervening matrix (Rumpel and Kögel-Knabner, 2010). Particularly in semi-arid vadose zones, these DOM-
 35 subsoil interactions occur in a context of frequent wet-dry cycles. Although such cyclic conditions likely impact C
 36 dynamics, the nature of their effects on micro- to molecular-scale organo-mineral associations remains poorly
 37 known.

38 The principal chemical mechanisms affecting DOM retention at soil particle surfaces – including ligand
 39 exchange with surface hydroxyl groups, ion-exchange of organic moieties at charged sites, cation bridging,
 40 hydrogen bonding and Van der Waals interactions depend on both DOM molecular composition and mineral
 41 surface chemistry (Chorover and Amistadi, 2001; Gu et al., 1994; Kleber et al., 2007, 2014). Interactions of DOM
 42 with dissolved polyvalent cations (e.g. Fe^{3+} and Al^{3+}) may also result in its coagulation and co-precipitation with
 43 nucleating metal (oxy)hydroxides (Chen et al., 2014a; Eusterhues et al., 2011). Drying of OM-mineral complexes
 44 can affect the mode of interaction. These effects may include changing of adsorption mode and product surface
 45 chemistry. For example, drying can convert OM adsorbate from outer- to inner-sphere coordination (Kang et al.,
 46 2008), promote exposure of hydrophobic functional groups of the adsorbed species, and increased surface catalysed
 47 transformation reactions (Olshansky et al., 2014). For systems where cation bridging plays a prominent role in
 48 DOM adsorption (e.g., to the siloxane surfaces of 2:1 layer type clay minerals), cation charge and valence effects
 49 are important, with increasing exchangeable Ca^{2+} relative to Na^{+} resulting in greater DOM retention (Setia et al.,
 50 2013).

51 Due to the heterogeneous nature of both DOM and soil mineral constituents, fractionation of DOM occurs
 52 as a result of a gradient of interaction affinities between the DOM components and various soil particle surfaces
 53 (Kaiser et al., 1997; Oren and Chefetz, 2012a). DOM fractionation has been studied extensively on single mineral
 54 phases (Chorover and Amistadi, 2001; Vazquez-Ortega et al., 2014) and on bulk soils (Guo and Chorover, 2003;
 55 Kaiser et al., 1997; Oren and Chefetz, 2012b). Metal (oxy)hydroxides have been suggested as a dominant adsorbent



for DOM with the result being preferential retention of high molar mass aromatic and carboxylated moieties (Chorover and Amistadi, 2001; Vazquez-Ortega et al., 2014). Conversely, layered silicates (e.g., smectites, kaolinite) were reported to adsorb mainly low molar mass and aliphatic DOM fractions (Chorover and Amistadi, 2001; Polubesova et al., 2008). While the use of specimen mineral phases in adsorption experiments facilitates elucidation of molecular mechanisms of DOM interaction, it does not account for the complexity of competitive interactions associated with heterogeneous assemblies of weathered surfaces as found in natural soils. Conversely, using whole soils in adsorption experiments has traditionally hindered mechanistic interpretations of DOM uptake results. However, increased spatial resolution of spectroscopic methods has helped to overcome these shortcomings by providing micro- and nano-scale information on both soil-mineral phases and associated organic molecules (Chen et al., 2014b).

The current study aimed to utilize such methodological advances to elucidate: (i) how wet-dry cycles affect the reactions between DOM and subsoil particle surfaces, and (ii) whether spatial fractionation of DOM is detectable with nanoscale resolution spectroscopic methods. We hypothesized that discontinuous wet-dry cycling during DOM reaction with subsoils would increase complexation of carboxyl groups with metal (oxy)hydroxide surfaces or hydroxylated edge surfaces of aluminosilicate clays and promote association of hydrophobic fractions with pre-adsorbed and desiccated DOM components relative to a continuous-wet condition. Such wetting-drying episodes have been hypothesized to affect organic carbon dynamics in water-limited portions of the critical zone, such as those that occur in the semi-arid southwestern US (Miller et al., 2005; Perdrial et al., 2014), but they have not been previously investigated in controlled laboratory experiments.

2 Materials and Methods

2.1 Soil samples

Soils were sampled from below mixed conifer forest in the Santa Catalina Mountains (SCM) and Jemez River Basin (JRB) Critical Zone Observatories (CZO) in Arizona and New Mexico, respectively (Chorover et al., 2011). The JRB soil was collected from the south slope of the San Antonio Mountain (35°55'10"N, 106°36'52"W) at an elevation of 2750 m. The SCM soil was collected from the northeast slope of the zero order basin located in the Marshall Gulch experimental site (32°25'44"N, 110°46'14"W) at elevation of 2600 m. The mean annual temperature is 6 and 10.4 °C for the JRB and SCM sites respectively. Both sites are subjected to bimodal annual precipitation patterns with averages of 850 and 940 mm y⁻¹. Parent rock is igneous felsic at both sites; granitic in the SCM and rhyolitic in the JRB. Therefore, the soils used in experiments developed under similar vegetation and



climatic condition but in different parent materials. The SCM and JRB soils are classified as Typic Ustorthents and Mixed Psammentic Cryoboralfs, respectively (Soil Survey Staff, 2010, USDA-NRCS., 1999). Soils were collected from the litter layer (0-2 cm) and Bw3 horizon (80-100 cm), from pedons excavated in April 2012 and October 2015 for SCM and JRB respectively. The SCM litter layer was collected in October 2015. Soils were air dried and sieved to obtain the fine earth (< 2 mm) fraction and stored in a closed container. Table 1 presents the bulk properties of the studied subsoils as measured using standard methods (Sparks, 1996). The mineral assemblages of both soils were dominated by quartz, feldspars and aluminosilicate clays (Table S1). The SCM soil had higher OM content (1.1 ± 0.5 mg C mg^{-1}) and lower pH (6.1 ± 0.04) than the JRB soil (0.17 ± 0.2 mg C mg^{-1} and 7.05 ± 0.11).

2.2 Dissolved organic matter extraction

The extraction of DOM was achieved by mixing the air-dried and sieved JRB or SCM litter with ultrapure water (1:5 g/g), and placing the suspension on a reciprocal shaker at 150 rpm for 24 h. Suspensions were centrifuged at 15,000 g for 30 min to separate the solids, using polypropylene copolymer (PPCO) centrifuge bottles. Adsorption or contamination of DOM from these bottles was measured to be negligible (Vazquez-Ortega et al., 2014). The supernatant solution was transferred into 50 mL PPCO centrifuge tubes and centrifuged again at 40,000 g for 20 min to remove colloidal organic material and the inorganic clay fraction. Supernatant solutions were filtered through pre-combusted and cleaned 0.7 μm glass fiber filters. TOC was measured immediately after extraction (Shimadzu TOC-VCSH, Columbia, MD) and solutions were diluted using ultrapure water to give initial DOC concentrations of 45 mg L^{-1} (Table 1). DOM solutions were stored at 4°C prior to use.

2.3 Sequential batch experiments

To model the effect of sequential hydrologic events delivering litter leachate to subsoils in the two CZO sites, subsoils were reacted in a set of four steps with DOM extracted from the litter layer of the corresponding profile. Thirty mL aliquots of DOM ([DOC] = 45 mg L^{-1}) solution were mixed with 3.0 g of soil in 50 mL PPCO centrifuge tubes and agitated (150 rpm, orbital shaker) at room temperature, in the dark. Preliminary kinetic experiments indicated an apparent equilibration time of 98 h, and this was chosen as the equilibration time for each reactor vessel. Suspensions were centrifuged for 30 min at 40,000 g and 28 mL were filtered through precombusted 0.7 μm glass fiber filters and the solutions were stored at 4 °C for a maximum of 24 h prior to analysis, as discussed below. For *continually-wet* treatments, a fresh 28 mL aliquot of DOM solution was added to each tube and suspensions agitated for an additional 98 h (28 mL were used because ca. 2 mL remained as entrained solution in the wet soil paste). For *wet-dry* treatments, the soil pastes were air dried for 24 h (drying was accomplished by



114 directing a low-flow circulating dry-air stream to promote desiccation), then an aliquot of 30 mL DOM solution
 115 was added to each tube and suspensions were re-agitated for 98 h, for a total of four sequential reaction cycles.
 116 Three replicates were prepared for each soil and treatment combination. After the four sequential reaction cycles,
 117 soils were freeze-dried and TOC and TN were measured using ECS 4010 CHNSO Analyzer (Costech, MI, Italy).
 118 During the experiment samples were maintained under oxic condition by equilibration with oxygenated headspace.

119 **2.4 Characterization of DOM solutions before and after reaction**

120 Reacted and unreacted DOM solutions were characterized by the following suite of complementary analytical
 121 methods: soluble TOC and TN were determined by total elemental analyzer (Shimadzu TOC-L and TNM-L,
 122 Columbia, MD), absorbance spectra (190 to 655 nm) were collected using a UV-Vis spectrometer (Shimadzu
 123 Scientific Instruments UV-2501PC, Columbia, MD, USA), fluorescence excitation–emission matrices (EEM) were
 124 obtained with a FluoroMax-4 equipped with a 150 W Xe-arc lamp source (Horiba Jobin Yvon, Irvine CA, USA),
 125 and Fourier transform infrared (FTIR) spectra were collected using a Nicolet NEXUS 670 IR spectrometer
 126 (Madison, WI). The EEMs were acquired with excitation (Ex) from 200 to 450 nm and emission (Em) from 250
 127 to 650 nm in 5 nm increments. Spectra were collected with Ex and Em slits at 5- and 2-nm band widths,
 128 respectively, and an integration time of 100 ms. Ultrapure water blank EEMs were subtracted and fluorescence
 129 intensities were normalized to the area under the water Raman peak, collected at excitation 350 nm. Additionally,
 130 an inner-filter correction was performed based on the corresponding UV–Vis scans (Murphy et al., 2013).
 131 Transmission FTIR spectra were collected with a KBr beam splitter and a deuterated triglycine sulfate (DTGS)
 132 detector. Aliquots of two mL of JRB DOM solutions were transferred onto IR transmissive Ge windows, dried
 133 under vacuum for 19 h, and spectra collected in transmission mode. For SCM DOM, 2 mL aliquots were freeze
 134 dried and mixed with IR-grade KBr, then compressed into pellets. For each sample, 120 scans were collected over
 135 the spectral range of 400–4000 cm^{-1} at a resolution of 4 cm^{-1} . Clean Ge windows and KBr pellets were used as
 136 background.

137 **2.5 Scanning Transmission X-ray Microscopy and Near Edge X-ray Adsorption Fine Structure (STXM- 138 NEXAFS) analysis of soils**

139 STXM-NEXAFS analyses were conducted on clay-size isolates to avoid particulate organic matter and to overcome
 140 possible alteration of C speciation during preparation of thin sections (Chen et al., 2014b). Clay size fractions (<2
 141 μm) of the reacted and unreacted JRB soils were separated by sedimentation after dispersion in ultrapure water
 142 using a sonication bath. Samples for STXM analysis were prepared by depositing 5 μL of diluted aqueous



suspension onto a Si₃N₄ window (75 nm thick) and air-dried. The samples were analyzed by STXM on beamline 10ID-1 at the Canadian Light Source (CLS), a 2.9 GeV third-generation synchrotron source. The microscope set up used a 25 nm Fresnel zone plate, which provided a maximum spatial resolution of *ca.* 30 nm. Samples were kept under 1/6 atm of He during measurement.

Spatially resolved spectra obtained by collecting stacks of images at energies below and above C 1s, Ca 2p, Fe 2p, element edges. The dwell time was set to 1 ms and pixel sizes of 150 nm. Incident energy was calibrated with CO₂ at 290.74 eV.

The aXis2000 software package (Hitchcock et al., 2012) was used for STXM image and spectral processing. Stacks were aligned and converted to optical density using a clean area of the Si₃N₄ window for normalization. Regions of interest (ROI) of C, Ca and Fe were extracted from each stack by subtracting below the edge from the optical density (OD) maps. C NEXAFS spectra were extracted by averaging the pixels from the ROI. NEXAFS spectra were normalized and peak deconvolutions were performed using the ATHENA software package (Ravel and Newville, 2005). Peak assignments were based on Cody et al. (1998, 2008), Myneni (2002) and Urquhart et al. (1997).

2.6 Data analysis

Statistical analyses were performed using *R* software packages (Mangiafico, 2016). Data were checked for normality and equal variance. Means were tested using Kruskal–Wallis for non-parametric analysis. The differences between means were examined using Dunn test for non-parametric analysis.

The specific UV absorbance (SUVA₂₅₄) was calculated by normalizing absorbance at incident wavelength 254 nm by the cell path length (1 cm) and DOC concentration (M). Fluorescence index (FI, Eq. 1) and humification index (HIX, Eq. 2) values were calculated from the corrected EEMs (McKnight et al., 2001; Ohno, 2002) as follows:

$$FI_{Ex370} = \frac{I_{450}}{I_{500}} \quad (1)$$

$$HIX_{Ex255} = \frac{\sum(I_{435 \rightarrow 480})}{\sum(I_{300 \rightarrow 345})} \quad (2)$$

where Ex is the excitation wavelength (nm) and *I* is the fluorescence intensity at each wavelength.



168 Spectra collected by FTIR were background corrected using KBr pellets or the Ge transmission window
 169 as blanks and baseline corrected using the spline function in the OMNIC 8 software program (Thermo Nicolet Co.,
 170 Madison, WI). Peak positions were determined using the second-order Savitzky–Golay method. Voigt line shape,
 171 (a convolution between mixed Gaussian and Lorentzian line shapes) were fitted to the peaks in the 850–1850 cm^{-1}
 172 region using Grams/AI 8.0 spectroscopy software (Thermo Electron Corporation). Peak assignments were based
 173 on Socrates (2004), Mayo et al. (2004), Omoike and Chorover et al. (2004) and Abdulla et al. (2010).

175 3. Results

176 3.1 Total Carbon and Nitrogen

177 The loss of DOC from solution per unit mass of soil was largely independent of reaction step and treatment. The
 178 mass loss of DOC upon reaction with SCM soil was 156 ± 5 , 217 ± 3 , 167 ± 17 , and $192 \pm 10 \text{ mg kg}^{-1}$ for steps 1–
 179 4, respectively, in the wet-dry treatment, and 163 ± 3 , 222 ± 4 , 217 ± 2.5 , and $214 \pm 6 \text{ mg kg}^{-1}$ in the continuously-
 180 wet treatment. The mass loss of DOC upon reaction with JRB soil was 248 ± 19 , 257 ± 1 , 197 ± 5 , and 200 ± 12
 181 mg kg^{-1} for steps 1–4, respectively, in the wet-dry treatment, and 256 ± 7 , 236 ± 26 , 176 ± 44 , and $208 \pm 2 \text{ mg kg}^{-1}$
 182 in the continuously-wet treatment. Hence, the mean fraction of OC removed from DOM solution was $58 \pm 5 \%$
 183 (SD) after each reaction step with JRB soil and OC uptake values were not significantly different between the
 184 continuously-wet and wet-dry treatments. In the SCM soil, the mean fraction of OC removed was $41 \pm 4\%$ of the
 185 total after each reaction step in the wet-dry treatment. In contrast to the other three treatments, the continually-wet
 186 SCM treatment indicated increasing amounts of OC removed in each step, with $39 \pm 0.8\%$ in the first step, $48 \pm$
 187 1% in the second, and $56 \pm 1\%$ in the third and fourth steps (Figure 1). At the end of four reaction steps the TOC
 188 of JRB soils increased from $1,700 \pm 74 \text{ mg OC kg}^{-1}$ for the unreacted soil to $2,750 \pm 87 \text{ mg OC kg}^{-1}$ and $2,840 \pm$
 189 99 mg OC kg^{-1} for the wet-dry and continuous-wet treatments respectively (Figure 1). For the JRB soil, increases
 190 in solid phase organic C are in close agreement with the cumulative amounts of DOC removed from reacted
 191 solutions (902 ± 26 and $876 \pm 34 \text{ mg OC kg}^{-1}$ for wet-dry and continuous-wet treatments respectively) and represent
 192 a 60% increase in soil TOC. Conversely, for the SCM soil, despite comparable cumulative losses from solution
 193 (733 ± 29 and $817 \pm 2 \text{ mg OC kg}^{-1}$ for wet-dry and continuous-wet treatments respectively), solid phase analyses
 194 indicated that the OC content of the reacted SCM ($11,200 \pm 380$ and $11,200 \pm 290 \text{ mg OC kg}^{-1}$ soil for wet-dry and
 195 continuous-wet treatments respectively) soils were effectively unchanged relative to the unreacted control ($11,800$
 196 $\pm 180 \text{ mg OC kg}^{-1}$).



197 Patterns in the removal of total N from the DOM solutions showed similar trends for both soils. In the first
 198 two wet-dry steps, a higher proportion of TN was removed from the solution (65 - 70% and 50 - 66% for SCM and
 199 JRB soils, respectively) than in the third and fourth steps (31 - 44% for both soils). The measured increase in soil
 200 TN by the end of the experiment were 63 and 143 mg N kg soil⁻¹ for SCM and JRB soils respectively. These values
 201 are slightly higher than the sum of TN removed from the solution (51 and 88 mg N kg soil⁻¹ for SCM and JRB soils
 202 respectively) (Figure 1).

203 The C:N ratio for all reacted DOM solutions decreased from step 1 to step 4, indicating preferential loss of
 204 C from solution, with no significant difference between the continually-wet and wet-dry treatments. However, after
 205 the first reaction with the SCM soil, the C:N ratio was 22.0 ± 1.3 , which was higher than the unreacted DOM (14.1
 206 ± 0.8). It is important to note that DOM extracted from unreacted soil had a C:N ratio of 23.7 ± 0.9 , and C:N of
 207 DOM decreased during the sequential reaction steps. After the fourth reaction step, ratios of 11.1 ± 0.8 and $9.6 \pm$
 208 0.8 were observed for the wet-dry and the continually-wet treatments respectively. The C:N of the reacted DOM
 209 solution with JRB soil decreased from 10 ± 1.0 after the first reaction step to 4.6 ± 0.5 after the fourth reaction step.
 210 The C:N ratio of unreacted DOM solution was 8.4 ± 0.8 . The overall change in soil C:N ratio was evaluated by the
 211 differences between unreacted soil and soils reacted four times with DOM solutions (Figure 1). Reacted SCM soils
 212 had significantly lower C:N (24.2 ± 1) than unreacted SCM soil (30.5 ± 1.8). However, no change in C:N was
 213 detected for reacted versus unreacted JRB soils.

214 3.2 UV-Vis and Fluorescence Spectroscopy

215 Reaction with subsoils altered spectroscopic properties of the litter-derived DOM solutions as reflected in UV-Vis
 216 (SUVA₂₅₄) and fluorescence indices (HIX and FI), and there was relatively little variation between continually-wet
 217 and wet-dry treatments (Figure 2). For both JRB and SCM the SUVA₂₅₄ values of DOM decreased (relative to
 218 unreacted DOM) upon contact with soil (Figure 2), with the exception of the fourth step in wet-dry treatment of
 219 SCM soil (Figure 2). This effect of contact with soil on SUVA₂₅₄ was larger for JRB than SCM, although it
 220 decreased with progressive reaction steps even for JRB soils from *ca.* 200 (L mol⁻¹ cm⁻¹) in the first step to *ca.* 50
 221 (L mol⁻¹ cm⁻¹) by the fourth step. High SUVA₂₅₄ (905 ± 35 L mol⁻¹ cm⁻¹) was measured for DOM extracted from
 222 unreacted JRB soil (Table 1). We note that SUVA₂₅₄ values of unreacted DOM also decreased between the first
 223 (393 L mol⁻¹ cm⁻¹) and subsequent steps (~ 350 L mol⁻¹ cm⁻¹) indicating some alteration of DOM chromophores in
 224 the stock DOM solution during the experiment. Although this was a small change relative to soil reaction effects,
 225 alteration was also evident in the HIX of unreacted JRB DOM. Therefore, treatment effects (continuous-wet and
 226 dry-wet) were evaluated on the basis of differences between reacted and unreacted solutions for the same reaction



step. The effect of reaction with soil on $SUVA_{254}$ values were less pronounced for SCM relative to JRB soils. In the wet-dry treatment of SCM soil, $SUVA_{254}$ values of the first three steps were generally consistent at $ca. 330 \pm 13$ ($L \text{ mol}^{-1} \text{ cm}^{-1}$) and in the fourth step the $SUVA_{254}$ increased to 530 ± 2 ($L \text{ mol}^{-1} \text{ cm}^{-1}$). Conversely, $SUVA_{254}$ values increased slightly over the course of the experiment from 324 ± 10 to 410 ± 16 $L \text{ mol}^{-1} \text{ cm}^{-1}$ for the continually-wet SCM treatment.

Humification index (HIX) values for the reacted DOM were generally higher or similar to the unreacted DOM (Figure 2). As with the $SUVA_{254}$ index, the fourth step of SCM wet-dry treatment was the exception (Figure 2), giving a lower HIX for reacted compared to unreacted DOM. The HIX values for DOM reacted with JRB soil were similar for continually-wet and wet-dry treatment. Conversely, with SCM soil, values for the wet-dry treatments were lower than for continually-wet treatments. The relative differences between reacted and unreacted DOM were lower for the JRB system than for the SCM system. For both JRB and SCM soils, higher fluorescence index (FI) values were observed for reacted relative to unreacted DOM (Figure 2) whereas wet-dry versus wet-only treatment effects were negligible. For JRB, FI values increased from 1.31 ± 0.04 (unreacted DOM) to 1.53 ± 0.04 whereas corresponding values for SCM were 1.34 ± 0.04 and 1.42 ± 0.02 , respectively. All FI values are in close agreement with the value of DOM associated with predominantly plant material ($ca. 1.4$), as opposed to microbial-derived DOM ($ca. 1.9$) (McKnight et al., 2001).

3.3 FTIR

Transmission FTIR spectra of reacted and unreacted DOM for the JRB and SCM systems are shown in Figures 3 and 4, respectively. The most prevalent peaks in the spectra were associated with amide I and II (1636 and 1560 cm^{-1} , respectively), carboxylate (asymmetric and symmetric stretches at 1592 and 1417 cm^{-1} , respectively), alkyl (CH_2 and CH_3 bending vibrations at 1455 and 1380 cm^{-1} , respectively), and aromatic moieties ($\text{C}=\text{C}$ ring vibration at 1500 cm^{-1} , phenol O-H bend 1370 cm^{-1}) and O-alkyl (CO^- stretch at 1030 - 1150 cm^{-1}).

For JRB soil, the first reaction step in both continually-wet and wet-dry treatments was accompanied by a decrease in peak intensities of carboxylate (1592 cm^{-1} and 1417 cm^{-1}) and amide (1636 and 1560) relative to O-alkyl (1150 - 1030 cm^{-1}). Additionally, primary alcohol (1035 cm^{-1}) peak intensity decreased relative to secondary alcohol (1100 cm^{-1}). This trend persisted in the second step with JRB soil for both treatments, although the pattern was less pronounced and differed by treatment. Specifically, the wet-dry treatment showed a larger decrease in the asymmetric carboxylate stretch (1592 cm^{-1}) whereas the continuous-wet treatment showed a larger decrease in the amide I peak (1636 cm^{-1}). In the third step, the decrease in amide and carboxyl peaks relative to O-alkyl was not as pronounced for the wet-dry as it was in the continually-wet treatment. Finally, in the fourth step of the wet-dry



system, a pronounced decrease in amide and carboxyl peaks relative to O-alkyl was again observed, whereas it was not in the continually-wet treatment (Figure 3).

Figure 4 shows the spectra of reacted and unreacted DOM in the SCM system. The SCM DOM spectra show similar peaks as the JRB with the addition of carboxyl ($\text{C}=\text{O}$ stretch at 1720 cm^{-1}) and ester ($\text{C}=\text{O}$ stretch 1770 cm^{-1} and $\text{C}-\text{O}$ stretch 1265 cm^{-1}). Similar to the JRB system, after reaction with soil, the peaks associated with carboxyl, carboxylate and amide decreased relative to the O-alkyl peaks and this trend was more pronounced in the first step than in the subsequent steps. Similar to the JRB system, in the fourth step of the wet-dry treatment, a pronounced decrease in carboxyl, carboxylate and amide peaks was again observed relative to the O-alkyl peaks.

3.4 STXM-NEXAFS

Given limitations in beam time, synchrotron analyses were focused on the JRB soil because it showed larger carbon accumulation over the course of the experiment. Scanning transmission x-ray microscopy (STXM) images of C, Fe and Ca obtained for the isolated fine fraction of JRB soils reacted four times with DOM in wet-dry and continually-wet treatments are shown in Figures 5 and 6, respectively. The carbon signal was observed over all particle surfaces, from continually-wet and wet-dry treatments after four reaction steps. Locations of higher Fe and Ca content were observed for both treatments. Near edge x-ray absorption fine structure (NEXAFS) spectra extracted from C, Ca and Fe-rich regions of interest (ROI) of the STXM maps and C NEXAFS spectra of bulk unreacted soil and DOM are included in Figures 5 and 6. Spectra of the unreacted DOM consist of peaks representing aromatic ($1s \rightarrow \pi^*$ at 285.1 eV), alkyl ($1s \rightarrow 3p/\sigma^*$ at 287.5 eV), amide ($1s \rightarrow \pi^*$ at 288 eV), carboxyl ($1s \rightarrow \pi^*$ at 288.5 and 290 eV), O-alkyl ($1s \rightarrow \pi^*$ at 289.5 eV) moieties. The C NEXAFS spectra of unreacted soil show no strong peaks of amide, carboxyl and O-alkyl, similar to the unreacted DOM spectra. However, after four steps of reaction with DOM, soil from both continually-wet and wet-dry treatments exhibited greatly enhanced carboxyl and O-alkyl peaks relative to the unreacted soil. In the wet-dry treatment, the aromatic peak was absent. The O-alkyl peak was more pronounced for the continually-wet than for the wet-dry treatment. Additionally, the amide peak was suppressed in the reacted soil compared to the unreacted DOM, and for the wet-dry treatment this peak was absent and was not included in the fitted spectra (supplementary material). The C NEXAFS spectra of Ca and Fe enriched ROIs are similar to the average whole image spectra. However in the Ca ROI, the carboxyl peak intensity was enhanced relative to Fe ROI and the averaged whole image spectra. This carboxyl enhancement, which was absent in the unreacted soil, was most pronounced in the wet-dry treatment.

Variations in the C NEXAFS spectra of the reacted soils following each reaction step are displayed in Figure 7. After the first reaction step, intensities of the carboxyl and O-alkyl peaks were relatively increased. For



the continually-wet treatment, spectra collected following the second and third steps show an increase in alkyl and O-alkyl peaks, whereas this trend was less evident in the wet-dry treatment.

4. Discussion

Specific surface area (SSA) and OC content are dominant factors controlling sorption of DOM to soil. For comparable mineralogy, higher SSA tends to increase DOM sorption, while higher solid phase OC content suppresses it (Kaiser et al., 1997; Oren and Chefetz, 2012b). In addition, solution chemistry can control DOM-soil interactions. For example, low pH can neutralize weakly acidic OM functionalities, thereby decreasing electrostatic repulsion from negatively-charged surfaces, whereas bivalent cations such as Ca^{2+} can form bridging complexes between negatively-charged surface and DOM sites (e.g., Setia et al., 2013). Further, the presence of polyvalent metal cations in solution can promote precipitation of (meta-)stable OM-metal complexes (Kleber et al., 2014). In the current study, in spite of differences in soil constituents and DOM compositions deriving from the two distinct CZO sites, similar amounts of DOM were removed from solution with both JRB and SCM soils. The fact that OC did not accumulate in the SCM soil solid phase despite significant removal from solution suggests that decomposition and mineralization are dominant factors indicated in the removal of OC from the reacted SCM DOM solutions. Indeed, the pronounced decrease in C:N ratio of the reacted soil is consistent with microbial transformation of organic matter (German et al., 2011). Higher HIX for all SCM reacted samples, with the exception of the last step in the wet-dry treatment, further support OM transformation. Enhanced mineralization in the SCM relative to JRB soil may be related to its substantially higher native OC content (Table 1), which would preclude surface stabilizing interactions and support a significantly higher native heterotrophic microbial biomass. The relatively lower HIX value for the last step of wet-dry treatment coincide with higher SUVA_{254} . Since SUVA_{254} index is correlated with sample aromaticity (Weishaar et al., 2003), an increase in the aromatic peak in the FTIR spectra was expected. However, FTIR spectra show a relative increase in O-alkyl rather than the aromatic vibrations. It is possible that the decrease observed in 1550 to 1700 cm^{-1} region is mainly due to a decrease in carboxyl associated peaks rather than increased aromaticity. It is unclear if the removed fraction was exchanged with previously adsorbed OM or preferentially decomposed in the solution.

Conversely, significant DOM or soil organic matter decomposition was not observed for the JRB soil experiments, as evidenced from the C mass balance. Therefore, changes in reacted DOM composition can be attributed to preferential adsorption and exchange reactions. The increased FI value of the reacted DOM further suggests preferential adsorption of plant- relative to microbial-derived OM. The slight decrease in SUVA_{254} values



316 is also consistent with this observation, since polyphenols derived from lignin account for most of the aromaticity
317 in DOM.

318 Spectra from C-NEXAFS obtained for the JRB soil fine fraction corroborate the solution data obtained by
319 FTIR. A pronounced increase in the carboxyl peak (288.5 eV) after the first reaction step (Figure 7) is consistent
320 with the decreased intensity of carboxyl in the reacted DOM solutions (Figure 3). NEXAFS spectra collected after
321 the second and third steps of both treatments show additional increases in the O-alkyl (289.5 eV) and alkyl (287.5
322 eV) that corroborate the relative decrease in FTIR peak intensities for these functionalities. The fact that the
323 NEXAFS of the reacted JRB soils clearly shows a relative increase in the carboxyl peak from the third to the fourth
324 step in the wet-dry treatment (Figure 7), suggests that preferential adsorption of the carboxylic component was
325 facilitated by the pre-existing soil-DOM phases of the dried soil. Prior work has shown that soil drying may promote
326 conformational changes in pre-adsorbed DOM that promotes preferential desorption of O-alkyl relative to further
327 inner-sphere coordination of carboxyl components (Kang et al., 2008; Kang and Xing, 2007). Additional support
328 for the formation of inner-sphere carboxyl complexes is from the higher preferential adsorption of carboxyl over
329 amide as observed in FTIR spectra of wet-dry compared to continuous-wet treatments (Figure 3).

330 Due to the heterogeneous composition of soil surfaces and DOM, spatial fractionation of the adsorbed
331 carbon moieties was expected. Figures 5 and 6 show that in both wet-dry and continuously-wet treatments, regions
332 containing higher content of Fe and Ca can be distinguished. Interestingly, the carbon NEXAFS spectra of these
333 distinct locations are generally similar. It is important to note that low Fe spectral signals were detected over all of
334 the particle surfaces images with STXM. This may suggest that weathered surfaces of the soil, coated with a thin
335 layer of metal (Fe) oxides and organic matter, can smear out what might otherwise be observed as a spatial
336 fractionation at this scale (nm).

337 However, close inspection of the C spectra extracted from Fe and Ca enriched zones and whole particle
338 regions reveal that in samples treated with wet-dry steps, the amplitude of the carboxyl peak shows a relative
339 increase preferentially in the Ca enriched regions (Figure 5 and supporting information). This finding suggests that
340 cation bridging interactions are pronounced in stabilizing the carboxyl component in the studied soil. It is important
341 to note that the solution pH was close to 7, and therefore deprotonated carboxylate species were predominant in
342 the suspension. Regions of high Ca are likely associated with charged aluminosilicate surfaces hosting
343 exchangeable cations. The enhancement effect of drying on Ca-carboxylate complex formation can be related to
344 the tendency of the Ca^{2+} hydration shell to become more acidic upon drying (Sposito, 1984). As water molecules
345 are gradually removed during air drying, polarizing forces of the Ca^{2+} cation increases, enhancing the tendency of
346 hydration water to donate protons (Dowding et al., 2005). Therefore, upon drying, protonation of the carboxylate



347 functionality is expected. Protonation of carboxylate decreases the electrostatic repulsion from negatively charged
 348 clay surfaces and increases the overall interaction with clays. It is important to note that our studied soils are
 349 predominantly composed of silicate and aluminosilicate minerals and are relatively depleted in crystalline and short
 350 range order metal oxides.

351 5. Conclusion

352 Results of this study show that wet-dry cycles affect interactions between DOM and subsurface soils, in this case
 353 by enhancing the interactions between carboxyl functional group and soil surfaces. Interactions of these
 354 functionalities were dominated by Ca^{2+} bridging to soil surfaces. The data also demonstrate that nanoscale spatial
 355 fractionation of DOM on soil organo-mineral surfaces was diminished relative to what might be inferred from
 356 observations pertaining to DOM fractionation on specimen mineral phases. This is likely due to the heterogeneous
 357 composition of the weathered soil surfaces and passivation of the underlying mineralogy by metal oxide and OM
 358 films. Fractionation of DOM in solution was similar under wet-dry conditions for a soil that presented measureable
 359 decomposition of the DOM (SCM) as it was for a soil that did not show any detectable decomposition (JRB).
 360 This study provides direct evidence of the role of wet-dry cycles in the sorption reactions of DOM to a complex
 361 soil matrix. In the soil environment, where wet-dry cycles occur at variable frequencies from site to site and along
 362 the soil profile, different interactions between DOM and soil surfaces are expected. This wet-dry effect can partially
 363 explain the observation that carbohydrates predominate in subsoil horizons, where soil is less subjected to drying,
 364 whereas aromatic and carboxylic compounds are more prevalent in top soils, where wet-dry cycles are more
 365 frequent (Kaiser and Kalbitz, 2012). Our findings demonstrate the need to consider the effect of wet-dry cycles in
 366 studying the interactions between DOM and soil surfaces.

367
 368 **Acknowledgements:** This research was funded by the Binational Agricultural Research and Development
 369 (BARD) program, postdoctoral fellowship to Y. Olshansky grant no. FI-534-2015, and the National Science
 370 Foundation, grant no. EAR 13-31408, which supports the Catalina-Jemez Critical Zone Observatory. The STXM
 371 analysis described in this paper was performed at the Canadian Light Source beamline 10ID-1, which is supported
 372 by the Canadian Foundation for Innovation, Natural Sciences and Engineering Research Council of Canada, the
 373 University of Saskatchewan, the Government of Saskatchewan, Western Economic Diversification Canada, the
 374 National Research Council Canada, and the Canadian Institutes of Health Research. Thanks to Mary Kay Amistadi,
 375 Rachel Nadine Burnett and Prakash Dhakal for assistance with analysis.



376

377 **References**

- 378 Abdulla, H. A. N., Minor, E. C., Dias, R. F. and Hatcher, P. G.: Changes in the compound classes of dissolved
 379 organic matter along an estuarine transect: A study using FTIR and ^{13}C NMR, *Geochim. Cosmochim. Acta*,
 380 74(13), 3815–3838, 2010.
- 381 Chen, C., Dynes, J. J., Wang, J. and Sparks, D. L.: Properties of Fe-Organic Matter Associations via Coprecipitation
 382 versus Adsorption., *Environ. Sci. Technol.*, 48(23), 13751–9, 2014a.
- 383 Chen, C., Dynes, J. J., Wang, J., Karunakaran, C. and Sparks, D. L.: Soft X-ray spectromicroscopy study of mineral-
 384 organic matter associations in pasture soil clay fractions, *Environ. Sci. Technol.*, 48(12), 2014b.
- 385 Chorover, J. and Amistadi, M. K.: Reaction of forest floor organic matter at goethite, birnessite and smectite
 386 surfaces, *Geochim. Cosmochim. Acta*, 65(1), 95–109, 2001.
- 387 Chorover, J., Kretzschmar, R., Garica-Pichel, F. and Sparks, D. L.: Soil biogeochemical processes within the
 388 critical zone, *Elements*, 3(5), 321–326, 2007.
- 389 Chorover, J., Troch, P. a., Rasmussen, C., Brooks, P. D., Pelletier, J. D., Breshears, D. D., Huxman, T. E., Kurc, S.
 390 a., Lohse, K. a., McIntosh, J. C., Meixner, T., Schaap, M. G., Litvak, M. E., Perdrial, J., Harpold, A. and Durcik,
 391 M.: How Water, Carbon, and Energy Drive Critical Zone Evolution: The Jemez–Santa Catalina Critical Zone
 392 Observatory, *Vadose Zo. J.*, 10(3), 2011.
- 393 Cody, G. D., Ade, H., Wirick, S., Mitchell, G. D. and Davis, A.: Determination of chemical-structural changes in
 394 vitrinite accompanying luminescence alteration using C-NEXAFS analysis, *Org. Geochem.*, 28(7–8), 441–455,
 395 1998.
- 396 Cody, G. D., Ade, H., Alexander, C. M. O. D., Araki, T., Butterworth, A., Fleckenstein, H., Flynn, G., Gilles, M.
 397 K., Jacobsen, C., Kilcoyne, A. L. D., Messenger, K., Sandford, S. A., Tyliczszak, T., Westphal, A. J., Wirick, S.
 398 and Yabuta, H.: Quantitative organic and light-element analysis of comet 81P / Wild 2 particles using C-, N-, and
 399 O- μ -XANES, *Meteorit. Planet. Sci.*, 43(1/2), 353–365, 2008.
- 400 Dowding, C. E., Borda, M. J., Fey, M. V. and Sparks, D. L.: A new method for gaining insight into the chemistry
 401 of drying mineral surfaces using ATR-FTIR, *J. Colloid Interface Sci.*, 292(1), 148–151, 2005.
- 402 Eusterhues, K., Rennert, T., Knicker, H., Kogel-Knabner, I., Totsche, K. U. and Schwertmann, U.: Fractionation
 403 of organic matter due to reaction with ferrihydrite: Coprecipitation versus adsorption, *Environ. Sci. Technol.*, 45(2),
 404 527–533, 2011.



- 405 Eusterhues, K., Neidhardt, J., Hädrich, A., Küsel, K. and Totsche, K. U.: Biodegradation of ferrihydrite-associated
406 organic matter, *Biogeochemistry*, 119(1–3), 45–50, 2014.
- 407 Fontaine, S., Barot, S., Barré, P., Bdioui, N., Mary, B. and Rumpel, C.: Stability of organic carbon in deep soil
408 layers controlled by fresh carbon supply., *Nature*, 450(7167), 277–80, 2007.
- 409 Gu, B., Schmitt, J., Chen, Z., Liang, L. and McCarthy, J. F.: Adsorption and desorption of natural organic matter
410 on iron oxide: mechanisms and models., *Environ. Sci. Technol.*, 28(1), 38–46, 1994.
- 411 Guo, M. and Chorover, J.: Transport and fractionation of dissolved organic matter in soil columns, *Soil Sci.*, 168(2),
412 108–118, 2003.
- 413 Hitchcock, A., Hitchcock, P., Jacobsen, C., Zimba, C., Loo, B., Rotenberg, E., Denlinger, J. and Kneeder, R.: *aXis*
414 2000-Analysis of X-ray Images and Spectra, 2012.
- 415 Kaiser, K. and Kalbitz, K.: Cycling downwards – dissolved organic matter in soils, *Soil Biol. Biochem.*, 52, 29–
416 32, 2012.
- 417 Kaiser, K., Guggenberger, G., Haumaier, L. and Zech, W.: Dissolved organic matter sorption on subsoils and
418 minerals studied by ¹³C-NMR and DRIFT spectroscopy, *Eur. J. Soil Sci.*, 48(June), 301–310, 1997.
- 419 Kalbitz, K., Solinger, S., Park, J.-H., Michalzik, B. and Matzner, E.: Controls on the dynamics of dissolved organic
420 matter in soils: A review, *Soil Sci.*, 165(4), 277–304, 2000.
- 421 Kang, S. and Xing, B.: Adsorption of dicarboxylic acids by clay minerals as examined by in situ ATR-FTIR and
422 ex situ DRIFT., *Langmuir*, 23(13), 7024–7031, 2007.
- 423 Kang, S., Amarasingiwardena, D. and Xing, B.: Effect of dehydration on dicarboxylic acid coordination at
424 goethite/water interface, *Colloid. Surface. A*, 318(1–3), 275–284, 2008.
- 425 Kleber, M., Sollins, P. and Sutton, R. K.: A conceptual model of organo-mineral interactions in soils: self-assembly
426 of organic molecular fragments into zonal structures on mineral surfaces, *Biogeochemistry*, 85(1), 9–24, 2007.
- 427 Kleber, M., Eusterhues, K. and Keiluweit, M.: Mineral–Organic associations: formation, properties, and relevance
428 in soil environments, edited by D. Sparks, *Adv. Agron.*, 130, 1–140, 2014.
- 429 Lutzow, M. V., Kogel-Knabner, I., Ekschmitt, K., Matzner, E., Guggenberger, G., Marschner, B. and Flessa, H.:
430 Stabilization of organic matter in temperate soils: mechanisms and their relevance under different soil conditions -
431 a review, *Eur. J. Soil Sci.*, 57(4), 426–445, 2006.
- 432 Mangiafico, S. Summary and Analysis of Extension Program Evaluation in R, 2016.
- 433 Mayo, D. W., Miller, F. A. and Hannah, R. W. Course Notes on the Interpretation of Infrared and Raman Spectra,
434 John Wiley & Sons, Inc., Hoboken, NJ, USA., 2004.



- McKnight, D. M., E. W. Boyer, P. K. Westerhoff, P. T. Doran, T. Kulbe and Anderson, D. T.: Spectrofluorometric characterization of dissolved organic matter for indication of precursor organic material and aromaticity, *L&O*, 46(1), 38–48, 2001.
- Murphy, K. R., Stedmon, C. A., Graeber, D. and Bro, R.: Fluorescence spectroscopy and multi-way techniques. PARAFAC, *Anal. Methods*, 5(23), 6557, 2013.
- Myneni, S. C.: Soft X-ray spectroscopy and spectromicroscopy studies of organic molecules in the environment, *Rev. Mineral. Geochemistry*, 49(1), 485–579, 2002.
- Ohno, T.: Fluorescence inner-filtering correction for determining the humification index of dissolved organic matter, *Environ. Sci. Technol.*, 36(4), 2002.
- Olshansky, Y., Polubesova, T. and Chefetz, B.: Reconstitution of cutin monomers on smectite surfaces : adsorption and esterification, *Geoderma*, 232–234, 406–413, 2014.
- Omoike, A. and Chorover, J.: Spectroscopic study of extracellular polymeric substances from *Bacillus subtilis*: aqueous chemistry and adsorption effects., *Biomacromolecules*, 5(4), 1219–30, 2004.
- Oren, A. and Chefetz, B.: Sorptive and desorptive fractionation of dissolved organic matter by mineral soil matrices., *J. Environ. Qual.*, 41(2), 526–33, 2012a.
- Oren, A. and Chefetz, B.: Successive sorption-desorption cycles of dissolved organic matter in mineral soil matrices, *Geoderma*, 189–190, 108–115, 2012b.
- Perdrial, J. N., McIntosh, J., Harpold, A., Brooks, P. D., Zapata-Rios, X., Ray, J., Meixner, T., Kanduc, T., Litvak, M., Troch, P. a. and Chorover, J.: Stream water carbon controls in seasonally snow-covered mountain catchments: impact of inter-annual variability of water fluxes, catchment aspect and seasonal processes, *Biogeochemistry*, 118(1–3), 273–290, 2014.
- Polubesova, T. and Chefetz, B.: DOM-Affected Transformation of Contaminants on Mineral Surfaces: A Review, *Crit. Rev. Environ. Sci. Technol.*, 44(3), 223–254, 2014.
- Polubesova, T., Chen, Y., Navon, R. and Chefetz, B.: Interactions of hydrophobic fractions of dissolved organic matter with Fe(3+) - and Cu(2+)-montmorillonite., *Environ. Sci. Technol.*, 42(13), 4797–803, 2008.
- Ravel, B. and Newville, M.: ATHENA, ARTEMIS, HEPHAESTUS: Data analysis for X-ray absorption spectroscopy using IFEFFIT, *J. Synchrotron Radiat.*, 12(4), 537–541, 2005.
- Rumpel, C. and Kögel-Knabner, I.: Deep soil organic matter—a key but poorly understood component of terrestrial C cycle, *Plant Soil*, 338(1–2), 143–158, 2010.
- Setia, R., Rengasmy, P. and Marschner, P.: Effect of exchangeable cation concentration on sorption and desorption of dissolved organic carbon in saline soils., *Sci. Tot. Environ.*, 465, 226–232, 2013.



- 466 Socrates, G.: Infrared and Raman characteristic group frequencies: Tables and charts, 3rd ed., John Wiley & Sons,
467 Ltd, Chichester, UK., 2004.
- 468 Soil Survey Staff, (2010). Keys to Soil Taxonomy, 11ed. USDA- Natural Resources Conservation Service,
469 Washington, DC.
- 470 Sparks, D. L.: Methods of soil analysis, in Part 3: chemical methods, Soil Science Society of America, Madison,
471 WI., 1996.
- 472 Sposito, G.: The structure of water near clay mineral surfaces, in The surface chemistry of soils, pp. 47–77, Oxford
473 University Press, New York., 1984.
- 474 Urquhart, S. G., Hitchcock, a. P., Smith, a. P., Ade, H. and Rightor, E. G.: Inner-Shell Excitation Spectroscopy of
475 Polymer and Monomer Isomers of Dimethyl Phthalate, J. Phys. Chem. B, 101(96), 2267–2276, 1997.
- 476 USDA-NRCS. (1999). Soil survey geographic (SSURGO) database for Sandoval County area, New Mexico
477 (Includes parts of Los Alamos and Rio Arriba Counties). Fort Worth, TX.
- 478 Vazquez-Ortega, A., Hernandez-Ruiz, S., Amistadi, M. K., Rasmussen, C. and Chorover, J.: Fractionation of
479 Dissolved Organic Matter by (Oxy)Hydroxide-Coated Sands: Competitive Sorbate Displacement during Reactive
480 Transport, Vadose Zo. J., 2–13, 2014.
- 481 Vázquez-Ortega, A., Perdrial, J., Harpold, A., Zapata-Ríos, X., Rasmussen, C., McIntosh, J., Schaap, M., Pelletier,
482 J. D., Brooks, P. D., Amistadi, M. K. and Chorover, J.: Rare earth elements as reactive tracers of biogeochemical
483 weathering in forested rhyolitic terrain, Chem. Geol., 391, 19–32, 2015.
- 484 Weishaar, J. L., Aiken, G. R., Bergamaschi, B. A., Fram, M. S., Fujii, R. and Mopper, K.: Evaluation of specific
485 ultraviolet absorbance as an indicator of the chemical composition and reactivity of dissolved organic carbon,
486 Environ. Sci. Technol., 37(20), 4702–4708, 2003.
- 487 Zhao, P., Zavarin, M., Leif, R. N., Powell, B. A., Singleton, M. J., Lindvall, R. E. and Kersting, A. B.: Mobilization
488 of actinides by dissolved organic compounds at the Nevada Test Site, Appl. Geochemistry, 26(3), 308–318, 2011.
- 489
- 490
- 491



Table 1. Physico-chemical characteristics of the study soils

	JRB	SCM
Clay (%)	33.9	22.6
Silt (%)	27.7	38.4
Sand (%)	38.4	50.9
SSA ($\text{m}^2 \text{g}^{-1}$) ^a	16.6 ± 0.2	7.7 ± 0.1
CEC ($\text{mmol}_c \text{kg}^{-1}$) ^b	86.6 ± 4.2	61.3 ± 0.8
OC (%) ^c	0.17 ± 0.02	1.11 ± 0.5
pH ^d	7.05 ± 0.11	6.10 ± 0.04
EC ($\mu\text{S cm}^{-1}$) ^d	61.5 ± 26.6	36.8 ± 8.8
DOC (mg L^{-1}) ^d	3.59 ± 0.82	13.45 ± 1.30
DOM pH	6.97 ± 0.06	5.91 ± 0.11
DOM EC ($\mu\text{S cm}^{-1}$)	170.7 ± 10.2	84.1 ± 12.3
SUVA ($\text{L mol}^{-1} \text{cm}^{-1}$)	905 ± 35	539 ± 105
HIX ^e	1.5 ± 0.1	4.5 ± 2.3
FI _f	1.40 ± 0.04	1.43 ± 0.03

^a BET-N₂ Specific surface area

^b Cation exchange capacity

^c Organic carbon

^d Obtained in soil aqueous extract (1:10 with 8.2 MΩ, Barnstead water)

^e Humification index

^f Fluorescence index

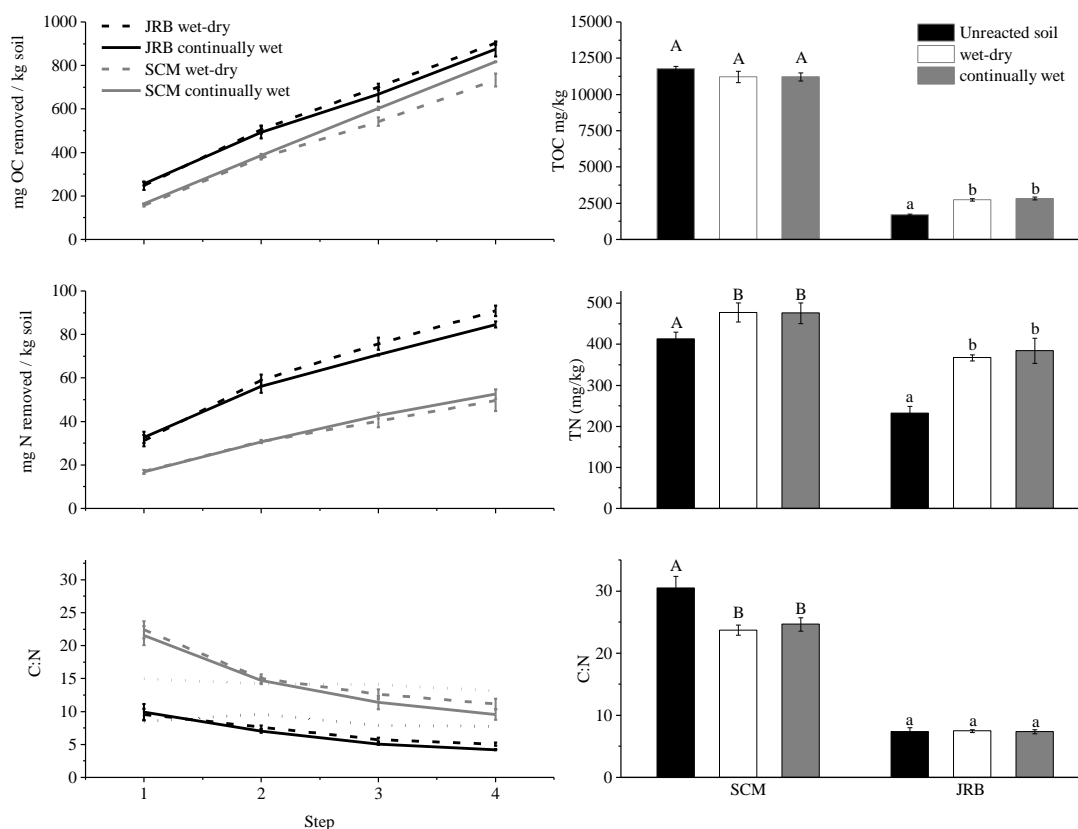
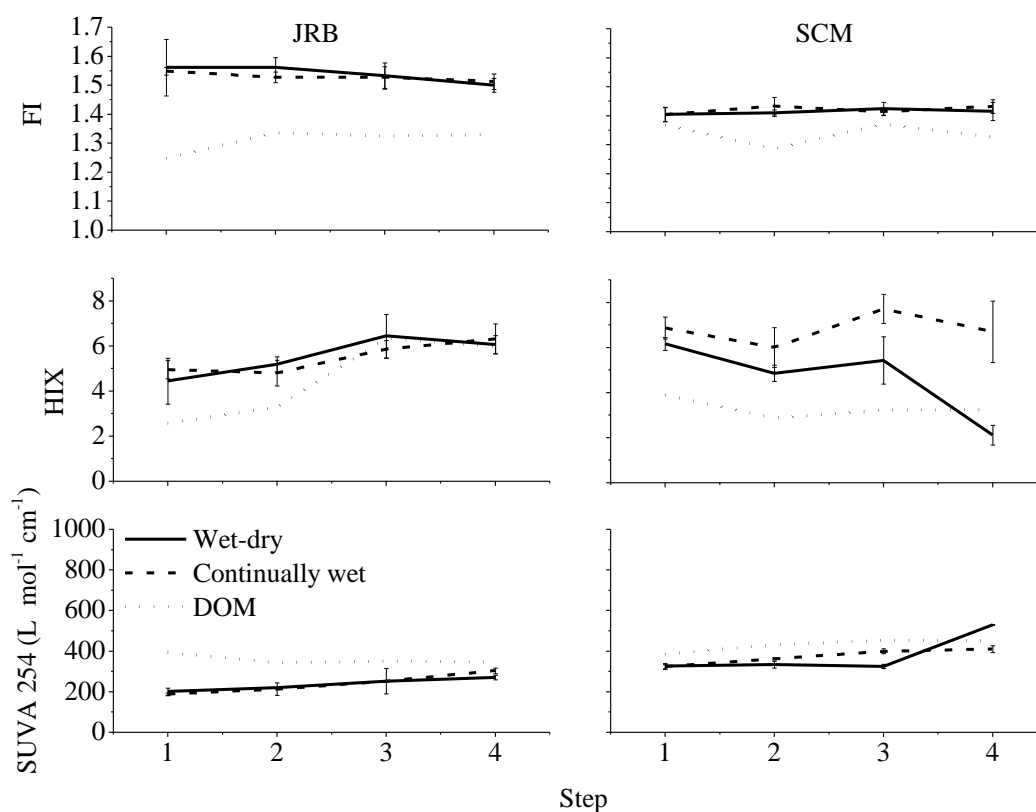


Figure 1: The organic carbon (top), nitrogen (middle) and C:N (bottom), for equilibrated solutions (left) and solid phases after four reaction steps (right). Values for equilibrated solution OC and N represent cumulative removal from solution per soil mass. Dashed lines in OC and N plots show continuous-wet treatments, dotted lines in the C:N plot represent values of unreacted DOM solutions, error bars are the standard deviation, and letters indicate significant difference ($p < 0.05$) from unreacted control.



512 **Figure 2. The fluorescence Index (FI), humification index (HIX) and specific UV absorbance at 245 nm (SUVA₂₅₄), for equilibrated**
 513 **solutions reacted with JRB and SCM soils. The solid lines are wet-dry series, dashed lines are continuous-wet, and dotted lines are**
 514 **unreacted DOM; error bars are the standard deviation.**

515

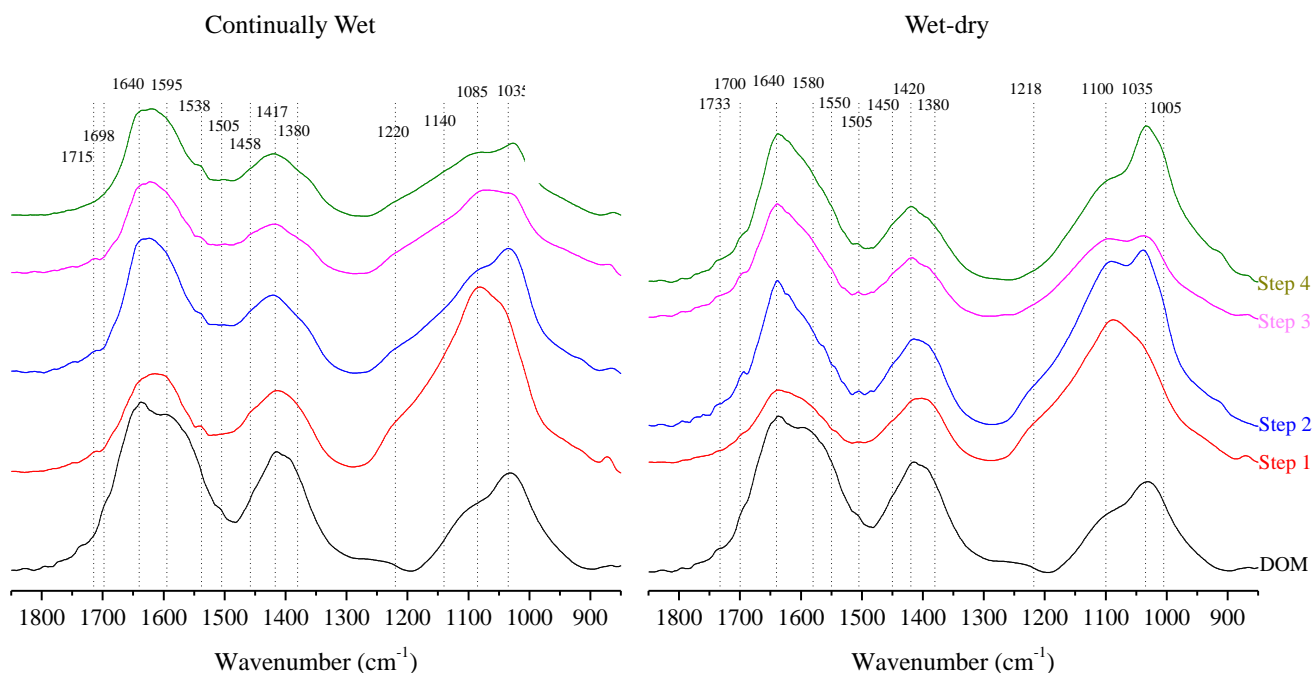
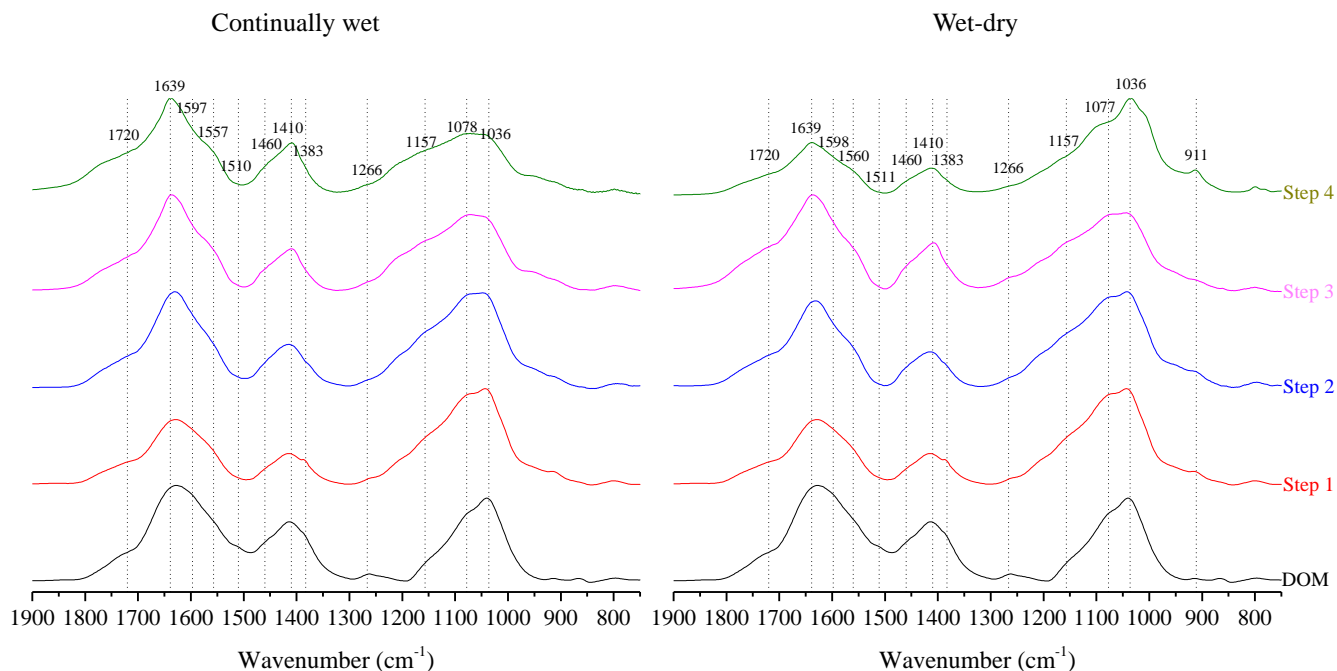


Figure 3. Transmission FTIR spectra of the DOM dried solution reacted with JRB soils from steps 1 to 4 for continuous-wet (left) and wet-dry cycled (right) and the unreacted JRB DOM solution (bottom black line). For color rendering of this image please refer to the online version.



524



525 **Figure 4. Transmission FTIR spectra of the DOM dried solution reacted with SCM soils from steps 1 to 4 for continuous-wet (left)**
 526 **and wet-dry cycled (right) and the unreacted SCM DOM solution (bottom line). For color rendering of this image please refer to**
 527 **the online version.**

528

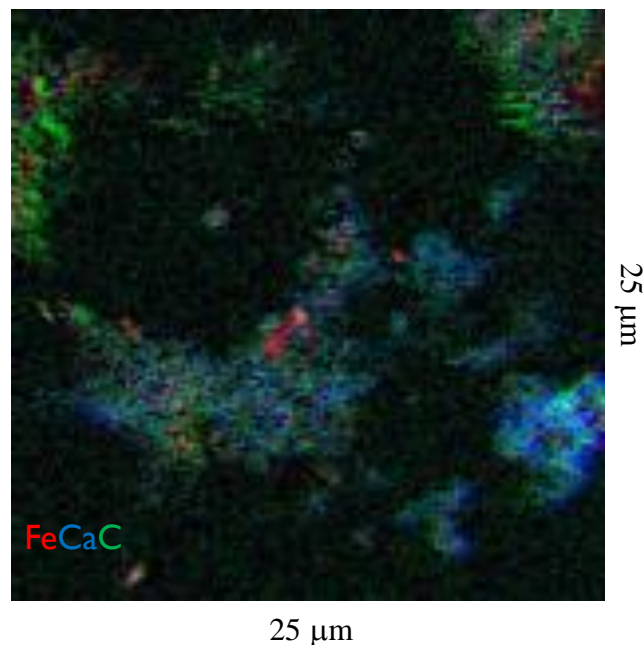
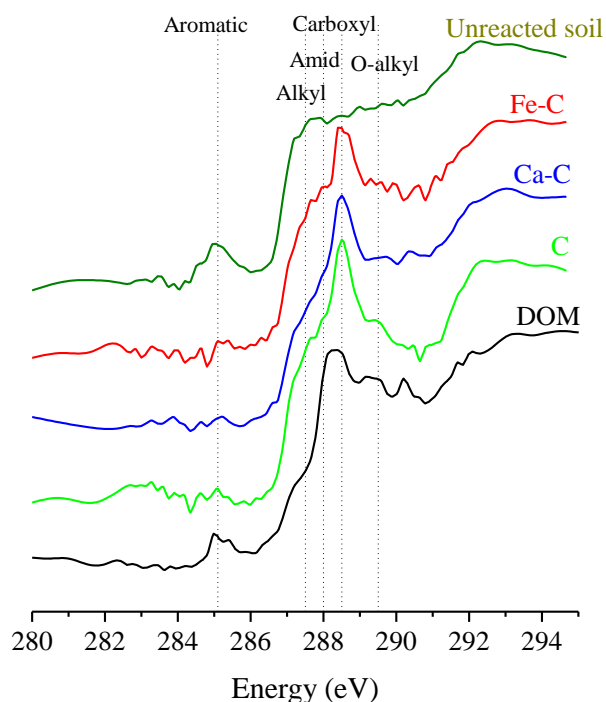
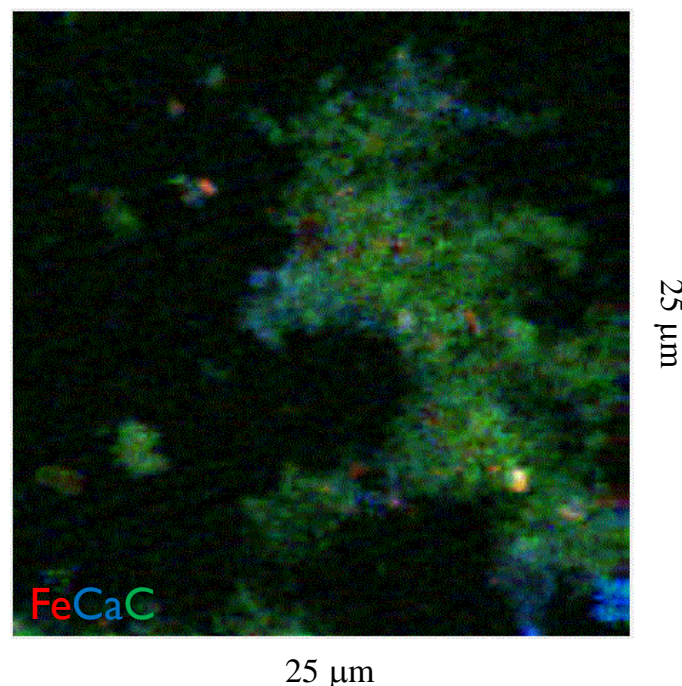
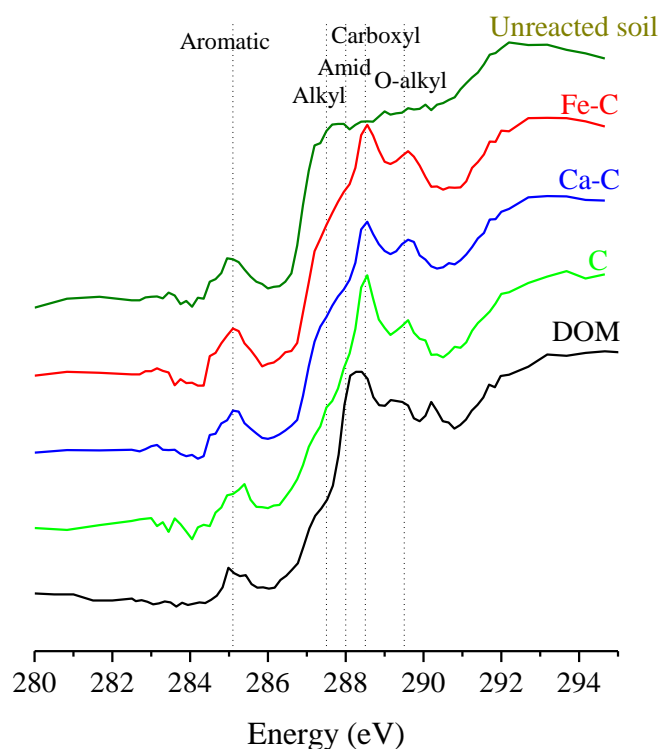


Figure 5. JRB soil reacted with DOM under wet-dry cycling. Left, C NEXAFS spectra extracted from C, Ca, and Fe regions of STXM map. Spectra of unreacted soil (top) and DOM solution (bottom) are presented. Dashed vertical lines point out C species. Right, tri-colored STXM map of fine fraction from JRB soil reacted four times with DOM under wet-dry cycling; Fe (red), Ca (blue) and C (green). Image size 25 x 25 μm . For color rendering of this image please refer to the online version.



536



537 **Figure 6. JRB soil reacted with DOM under continuous-wet conditions. Left, C NEXAFS spectra extracted from C, Ca, and Fe**
 538 **regions of STXM map. Spectra of unreacted soil (top) and DOM solution (bottom) are presented. Dashed vertical lines point out C**
 539 **species. Right, tri-colored STXM map of fine fraction from JRB soil reacted four times with DOM during the continuous-wet**
 540 **treatment. Fe (red), Ca (blue) and C (green). Image size 25 x 25 μm. For color rendering of this image please refer to the online**
 541 **version.**

542

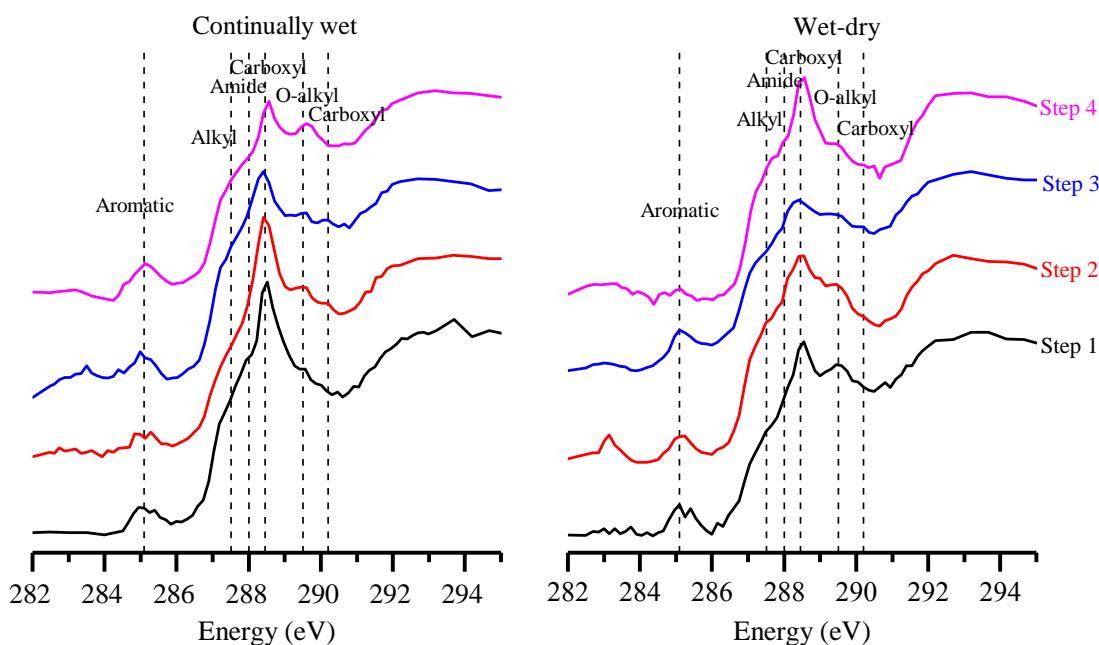


Figure 7. C NEXAFS extracted from C (red in Fig 6) regions of STXM map for the second step of the continuous-wet treatment (left) and from all 4 steps of the wet-dry treatment (right). For color rendering of this image please refer to the online version.